Optimized Dynamic Graph-Based Framework for Skin Lesion Classification in Dermoscopic Images

J. Deepa, P. Madhavan
Department of Computing Technologies, SRM Institute of Science and Technology, Kattankulathur, Chennai, India

***Abstract*—Early and accurate classification of skin lesions is critical for effective skin cancer diagnosis and treatment. However, the visual similarity of lesions in their early stages often leads to misdiagnoses and delayed interventions. This lack of transparency makes it challenging for dermatologists to interpret with validate decisions made by such methods, reducing their trust in the system. To overcome these complications, Skin Lesions Classification in Dermoscopic Images using Optimized Dynamic Graph Convolutional Recurrent Imputation Network (SLCDI-DGCRIN-RBBMOA) is proposed. The input image is pre-processed utilizing Confidence Partitioning Sampling Filtering (CPSF) to remove noise, resize, and enhance image quality. By using the Hybrid Dual Attention-guided Efficient Transformer and UNet 3+ (HDAETUNet3+) it segment ROI region of the preprocessed dermoscopic images. Finally, segmented images are fed to Dynamic Graph Convolutional Recurrent Imputation Network (DGCRIN) for classifying skin lesion as actinic keratosis, dermatofibroma, basal cell carcinoma, squamous cell carcinoma, benign keratosis, vascular lesion, melanocytic nevus, and melanoma. Generally, DGCRIN does not express any adaption of optimization strategies for determining optimal parameters to exact skin lesion classification. Hence, Red Billed Blue Magpie Optimization Algorithm (RBBMOA) is proposed to enhance DGCRIN that can exactly classify type of skin lesion. The proposed SLCDI-DGCRIN-RBBMOA technique attains 26.36%, 20.69% and 30.29% higher accuracy, 19.12%, 28.32%, and 27.84% higher precision, 12.04%, 13.45% and 22.80% higher recall and 20.47%, 16.34%, and 20.50% higher specificity compared with existing methods such as a deep learning method dependent on explainable artificial intelligence for skin lesion classification (DNN-EAI-SLC), multiclass skin lesion classification utilizing deep learning networks optimal information fusion (MSLC-CNN-OIF), and classification of skin cancer from dermoscopic images utilizing deep neural network architectures (CSC-DI-DCNN) respectively.**

***Keywords*—Confidence partitioning sampling filtering; dynamic graph convolutional recurrent imputation network; ISIC-2019 skin disease dataset; red billed blue magpie optimization algorithm; hybrid dual attention-guided efficient transformer and UNet 3+**

I. INTRODUCTION

Skin cancer is considered one of the most dangerous cancer types due to its high prevalence and potential for metastasis if not detected early. Melanoma, in particular, has a high mortality rate and can spread rapidly to other organs [1]. Statistics show that skin cancer is more common than other cancers, with rising incidence rates globally. Comparative studies also indicate that, although treatable when caught early, skin cancer has a higher likelihood of fatal outcomes compared to many other cancer types [2]. A skin lesion refers to abnormal appearance otherwise growth of skin analyzed to surrounding region [3]. Lesions can vary in color, type, shape, texture, position, distribution, they are categorized to classification prearranged hierarchically [4]. The first two major classifications of this hierarchy are melanocytic, non-melanocytic lesions [5]. The classification as melanocytic or non-melanocytic depends on presence or absence of melanocytes, melanin pigment in lesion [6]. Melanocytic lesions possess eight global features that assist in detailed categorization of pigmented skin lesions, along with fourteen local features provide more specific information about each lesion [7]. Hemoglobin causes non-melanocytic lesions to seem purple, red, blue, or black, while keratin causes them to appear orange or yellow [8]. These lesions can be either cancerous otherwise non-cancerous. Dermoscopic is commonly utilized skin imaging methods, aimed at enhancing diagnostic accuracy, reducing mortality from skin cancer [9]. This non-invasive method captures magnified with well-illuminated image of skin, allowing for a clearer examination of lesion area [10]. This method improves doctors' diagnostic ability and is typically used to detect skin cancer in its premature stages [11]. Dermatologists typically utilize visual examination to evaluate dermoscopic images, known as biomedical images [12]. It takes a lot of time, is labor-intensive, and is subject to operator bias. The reason for this is normal moles and skin infections can sometimes be so similar that a precise diagnosis might be challenging [13]. Several computer-aided diagnostic systems created to aid dermatologists identify skin cancer [14]. These methods not only get over the aforementioned problems but also increase the diagnosis system's impartiality, accuracy, and efficiency [15]. Deep learning approaches have established encouraging results, important promise in this area for data analysis and image processing [16]. Owing to its widespread use, distinctive characteristics in several complicated fields, likes object detection, classification, identification, and recognition, deep learning applied extensively [17]. The deep learning method gives method greater depth; changes input utilizing different functions enable hierarchical data representation across multiple levels of abstraction [18]. Because more sophisticated models are used, deep learning can quickly and effectively learn more difficult issues. The significant component of typical computer aided diagnostic systems is deep learning approaches like CNN and image processing techniques [19]. However, as processing cycle behind method learning with feature encoding is poorly implicit, utility of such computer-aided diagnostic systems by dermatologists, patients is still

questionable. Without a logical justification, the model prevents dermatologists from making informed decisions [20].

The problem involves in several existing methods, skin cancer at premature stage owing to challenges in analyzing dermoscopic images of skin lesions, which are often subtle and require a high level of expertise. Traditional visual inspection by dermatologists is time-consuming, subjective, and prone to error, making it hard to achieve consistent and reliable results. There is a need for automated systems that can assist in the accurate, efficient, and objective classification of skin lesions to enhance diagnostic accuracy, ultimately lessen skin cancer mortality.

This paper intends to overcome these issues to improve skin lesion detection methods, it is crucial to address the significant challenges that skin lesion. Enhancing the accuracy of identifying and classifying skin lesion detection is vital for facilitating timely and effective responses to these incidents. The suggested method attempts to improve detection accuracy and reliability by exploiting optimization using Red Billed Blue Magpie Optimization Algorithm.

The novelty of SLCDI-DGCRIN-RBBMOA method lies in its use of Skin Lesions Classification of Dermoscopic Images using Optimized Dynamic Graph Convolutional Recurrent Imputation Network. CPSF is used for preprocessing dermoscopic images, effectively removing noise and resizing them to improve image quality. The ROI region is segmented utilizing HDAETUNet3+, which improves the accuracy of lesion detection. The main innovation of the approach lies in the use of the DGCRIN for classifying a diverse range of skin lesions. The RBBMOA strategy significantly enhances accuracy, precision, recall, specificity, F1-score while also reducing error rate compared to existing methods, making it more suitable for classification on Skin Lesions in the future.

Major contribution of this investigate work is brief as below,

- To propose SLCDI-DGCRIN-RBBMOA framework, which employs an Optimized Dynamic Graph Convolutional Recurrent Imputation Network to enhance the Skin Lesions Classification of Dermoscopic Images process.
- Here, CPSF improves data integrity by efficiently for remove noise, resize and improve image quality within the dataset.
- To segment the ROI region using the Hybrid Dual Attention-guided Efficient Transformer and UNet 3+ (HDAETUNet3+) process and to classify Skin Lesion using DGCRIN, thereby improving classification accuracy.
- RBBMOA introduces an optimization approach to improve the weight parameters of the DGCRIN classifier.
- Performance comparison to analyze the efficiency of the SLCDI-DGCRIN-RBBMOA approach in comparison to well-known DGCRIN in context of Skin Lesion.

The proposed model addresses the limitations of previous approaches by enhancing transparency, accuracy, and optimization in skin lesion classification. To build trust in AI-based decisions, it incorporates Hybrid Dual Attention-guided Efficient Transformer and UNet 3+ (HDAETUNet3+), enabling precise segmentation and improved interpretability. Confidence Partitioning Sampling Filtering (CPSF) enhances image quality by eliminating noise, facilitating more accurate early-stage lesion classification and reducing diagnostic errors. The model leverages Transformer-based feature extraction and multi-scale segmentation to refine region of interest (ROI) identification, outperforming conventional deep learning methods. Furthermore, the Dynamic Graph Convolutional Recurrent Imputation Network (DGCRIN) captures spatial relationships within dermoscopic images, offering a structured and adaptive classification approach. Unlike previous graph-based models that lack effective parameter tuning, the Red Billed Blue Magpie Optimization Algorithm (RBBMOA) optimizes DGCRIN, significantly improving classification performance.

Remaining part of the paper is arranged as follows: Literature review is presented in Section II, Methodology employed is discussed in Section III, and result with discussion is described in Section IV and conclusion in Section V.

II. Literature Review

A. Related Work

Several investigate works are presented in literatures based on the Skin Lesion Classification utilizing Deep Learning. Table I presents various advantages and disadvantages of the existing Skin Lesion Segmentation and Classification model. In 2022, Nigar, N., et al., [21] have presented a Deep Learning approach based on Explainable Artificial Intelligence for skin lesion classification. A skin lesion classification system based on Explainable Artificial Intelligence is suggested to enhance the accuracy of skin lesion detection, aiding dermatologists in making more informed and rational diagnoses, particularly in the early stages of skin cancer. The system accurately identifies eight types of skin lesions: dermatofibroma, squamous cell carcinoma, benign keratosis, melanocytic nevus, vascular lesion, actinic keratosis, basal cell carcinoma, and melanoma. It attains high accuracy and low precision.

In 2024, Khan, M.A., et al., [22] have presented multiclass skin lesion classification utilizing deep learning networks optimal information fusion. A computerized method for multiclass skin lesion classification, leveraging a fusion of optimal deep learning model features is developed. The collection of data used in is unbalanced, thus mathematical operations are performed to address this problem through data augmentation. The augmented dataset is used to refine and train two pre-trained deep learning models, DarkNet-19 and MobileNet-V2. After training, features extracted from the average pooling layer are optimized using a hybrid firefly optimization technique. The selected features are then fused using both the threshold-based and serial approaches, and classified using machine learning classifiers. It attains higher recall and low specificity.

In 2023, SM, J., et al., [23] have presented classification of skin cancer from dermoscopic images using deep neural network architectures. A deep convolutional neural network (DCNN) model is developed to accurately classify melanoma and non-melanoma skin cancer. The datasets, sourced from various challenges, have issues like class imbalance and varying image resolutions. To address these, EfficientNet with transfer learning is used to capture more complex patterns by adjusting the network's depth, width, and resolution. The dataset is augmented, and metadata is incorporated to improve classification performance. Additionally, the EfficientNet model is optimized with the Ranger optimizer, reducing the need for extensive hyperparameter tuning. It provides high F1-score and high computational time in 2023, Alsahafi, Y.S., et al., [24] have presented Skin-Net, a novel deep residual network for skin lesions classification. It utilizes multilevel feature extraction and cross-channel correlation, along with outlier detection. In this suggested paper, the Residual Deep Convolutional Neural Network is designed with multiple convolutional filters for multi-layer feature extraction and cross-channel correlation, using sliding dot product filters instead of sliding filters along the horizontal axis. To address the problem of imbalanced datasets, the method transforms the dataset from image-label pairs to image-weight vectors. It has been tested and assessed on complex and demanding datasets and demonstrates superior performance compared to existing deep convolutional networks in multiclass skin lesion classification. It attains higher detection accuracy and low kappa coefficient.

TABLE I. STRENGTHS AND LIMITATIONS OF THE CURRENT MODELS FOR CLASSIFYING SKIN LESIONS

Authors Name	Methods	Advantage	Limitation
Nigar, N., et.al, [21]	Convolutional neural network, deep neural network	It achieves higher accuracy	It provides low precision
Khan, M.A., et.al, [22]	CNN, DarkNet-19, MobileNet-V2	It attains higher recall	It attains low specificity
SM, J., et.al, [23]	Deep neural network, DCNN, EfficientNet, DenseNet	It provides higher F1-score	It provides high computational time
Alsahafi, Y.S., et.al, [24]	Residual Deep CNN, DNN, Probabilistic neural network	It provides high detection accuracy	It provides low kappa coefficient
Raghavendra, P.V., et.al, [25]	Deep convolutional neural network, ResNet50, VGG-16, MobileNetV2, and DenseNet121	It attains higher RoC	It attain slow precision
Rezaee, K. et.al, [26]	Convolutional neural network, ResNet-50, and ResNet-101	It provides high specificity	It provides high loss function
Thanka, M.R., et.al, [27]	Generative adversarial network, VGG16 and XGBoost	It attains low error rate	It attains high sensitivity

In 2023, Raghavendra, P.V., et al., [25] have presented Deep Learning Based Skin Lesion Multi-class Classification with Global Average Pooling Improvement. The model is trained and tested on the dataset, which includes seven distinct classes of skin lesions. During the preprocessing stage, the black hat filtering technique is applied to remove artifacts, along with resampling techniques to address class imbalance. The performance of the proposed model is evaluated by comparing it with several transfer learning models, including ResNet50, VGG-16, MobileNetV2, and DenseNet121. It attains high RoC and low precision.

In 2024, Rezaee, K. et al., [26] have presented self-attention transformer based deep learning framework for skin lesions classification in smart healthcare. This approach fuses global and local features through cross-fusion to generate fine-grained features. The branches of the parallel systems are merged using feature-fusion architecture, creating a pattern that identifies the characteristics of various skin lesions. Additionally, the paper introduces an optimized and lightweight version of the CNN architecture, optResNet-18, designed to effectively discriminate between skin cancer lesions. It attains higher specificity and high loss function.

In 2023, Thanka, M.R., et al., [27] have presented hybrid technique for melanoma classification utilizing ensemble ML methods and deep transfer learning. A hybrid approach combining a pre-trained convolutional neural network and machine learning classifiers is employed for feature extraction and classification, enhancing the model's accuracy. VGG16 is used for feature extraction, while XGBoost serves as the classifier. This combination leverages the strengths of deep learning for feature extraction and the power of machine learning for efficient classification, leading to improved performance in skin lesion classification. It provides low error rate and low sensitivity.

B. Research Gap

Current skin lesion classification models suffer from a lack of transparency, reducing trust in AI-driven diagnoses. Early-stage lesion detection is challenging due to visual similarities. Existing methods struggle with accurate segmentation and feature extraction, while graph-based networks lack optimization. The proposed SLCDI-DGCRIN-RBBMOA improves classification through enhanced segmentation and advanced optimization strategies.

III. PROPOSED METHODOLOGY

The SLCDI-DGCRIN-RBBMOA methodology, which aims to classification of skin lesion, begins by input dermoscopic images are collected from ISIC-2019 skin disease dataset. The proposed block diagram of SLCDI-DGCRIN-RBBMOA is represented in Fig. 1. Input images are pre-processed with filtering to remove noise, improve image quality, followed by segmentation process, and are then fed into a classification process. The Dynamic Graph Convolutional Recurrent Imputation Network is then used to categorize the skin lesion as actinic keratosis, Dermatofibroma, Basal cell carcinoma, Squamous cell carcinoma, Melanocytic nevus, benign keratosis, Melanoma, vascular lesion. To improve classification accuracy, Red-Billed Blue Magpie Optimization Algorithm is utilized to enhance DGCRIN parameters. The overall system aims to detect, mitigate skin lesion, ensuring the integrity and reliability of image.

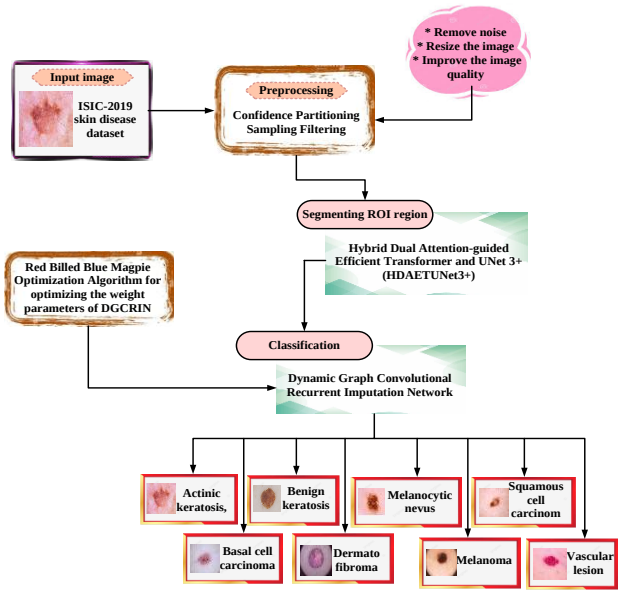

Fig. 1. Block diagram of SLCDI-DGCRIN-RBBMOA method.

A. Image Acquisition

The input data are gathered from ISIC-2019 Skin Disease Dataset [28]. This dataset comprises of 25,331 dermoscopic images, classified into eight types such as actinic keratosis, dermatofibroma, melanoma, benign keratosis, vascular lesion, basal cell carcinoma, melanocytic nevus, squamous cell carcinoma. The generated dataset is randomly splitted as 80% training, 10% testing, and 10% validation.

B. Pre-processing utilizing Confidence Partitioning Sampling Filtering

The image pre-processing utilizing CPSF [29] to eliminate noise, resize the image, and enhance image quality. CPSF methods were selected as a pre-processing technique for skin lesion analysis because they enhance image contrast, remove noise, and resize image, thereby improving the accuracy and clarity of lesion boundaries. This technique effectively reduces noise while preserving important features, enhancing the overall quality of segmentation. As a result, CPSF leads to more robust segmentation and better performance in subsequent analysis, providing more reliable results in dermoscopic images by reducing artifacts and noise. CPSF improves overall quality of images, enabling subsequent models, such as segmentation networks, to focus more effectively on relevant features and generate more accurate predictions. It also facilitates image resizing without sacrificing important details, which is particularly useful when working with datasets that require standardized input dimensions. Additionally, CPSF is a versatile tool that applied to different image types beyond dermoscopic images, making it valuable for medical image preprocessing as well as other computer vision applications. Then, the CPSF is given in Eq. (1),

$$w.k \int_{B_{q(y)}}^{\alpha} q(y)dx = 1 - \alpha \tag{1}$$

where, $q(y)$ represents the dimensional space, w denotes the hyper parameter, k represents the input data values, represents the filtering process, dx denotes the steady-state phase. Then, it is calculated as given in Eq. (2),

$$\omega_h = \frac{q(\hat{Y}_h)}{\sum_{h=1}^{H} q(\hat{Y}_h)} \tag{2}$$

Here, $q(\hat{Y}_h)$ represents the partitioning filtering of a distribution, ω_h denotes the bounded subspace, and H represents the sampling interval. It evaluates the correlations between features to predict quality images using variables that are strongly related.

Let qc represents the impulse function, y_t denotes the noise model, $\vec{y}_{t,c}$ represents the weighted grid samples, then image resize c is calculated using Eq. (3),

$$q(y_t | \hat{y}_{t-1,c}) = qc(y_t - \vec{y}_{t,c}) \tag{3}$$

It helps maintain the variation and structure of the original image, ensuring that the imputed values do not alter overall trends. In this step the denoise images are calculated as in Eq. (4),

$$\bar{y}_t = (\omega_t)^K \hat{y}_t \tag{4}$$

In the above equation, $\bar{y}_t$ represents the probability region, ω_t denotes the CPSF framework, $\hat{y}_t$ represents the denoise image. Then, the improved image quality is predicted as given in Eq. (5).

$$\vec{Y}_t = \left[\vec{y}_{t,1}, \vec{y}_{t,2}, ..., \vec{y}_{t,C_{t-1}}\right]^K \tag{5}$$

Here C_{t-1} represents the estimation of the prior CPSF, $\vec{y}_{t,1}$ represents the improved image quality, $\vec{y}_{t,2}$ denotes the local inference, $\vec{Y}_t$ denotes improved image quality. Here, by using CPSF method it remove noise, resize and improve image quality. After that, the pre-processed images undergoes segmentation phase.

C. Segmentation Using Hybrid Dual Attention-Guided Efficient Transformer and UNet 3+

Segmentation using HDAETUNet3+ [30, 31] method is to segment ROI region from dermoscopic images. The DAET and U-Net3+ is selected for its synergistic benefits in image segmentation. Dual attention mechanisms in DAET are highly effective at capturing long-range dependencies and fine-grained details, which are essential for precise segmentation. Meanwhile, Hierarchical structure and skip connections of U-Net3+ efficiently propagate contextual information across different scales, enhancing localization and boundary delineation. It enhances methods ability to exactly segment skin lesions, even with complex boundaries, by capturing both local and global features. This improves lesion classification and results in a more computationally efficient and robust method for skin lesion recognition in dermoscopic images.

Dual Attention-guided Efficient Transformer, which integrates spatial and channel attention, enables method to emphasis on the most applicable image regions and key features, resulting in accurate, robust segmentation of skin lesions. The architecture efficiently scales to learn large image sizes or long sequences, which is essential for tasks such as high-resolution medical image segmentation. By leveraging the attention mechanism, the model can adapt to a wide range of input data, including varying image sizes and resolutions, making it versatile for deployment across different applications. Additionally, the attention mechanism provides greater transparency into methods decision-making process, which is particularly valuable in high-stakes domains like medical imaging. Attention maps highlight areas the model prioritizes, offering insights into its focus during predictions and improving interpretability. It is given in Eq. (6).

$$R(P,K,U) = soft\max\left(\frac{PK^{S}}{\sqrt{c_k}}\right)U \tag{6}$$

Here, the term c is the embedding dimension, U is the value vector of the image. Conventional self-attention may produce redundant context matrix, effectual way to calculate self-attention mechanism is provided in Eq. (7).

$$F(P,K,U) = \rho_p(P)\left(\rho_k(K)^{S}U\right) \tag{7}$$

Here, ρ_p and ρ_k denotes normalization functions for queries, keys. These are softmax normalization functions. Hence, efficient attention first normalizes the keys and queries and then multiplies keys with values. The transpose attention is shown in Eq. (8).

$$MLP(Y) = FC\left(GELU\left(DW-Conv\left(FC(Y)\right)\right)\right) \tag{8}$$

In Eq. (8), MLP represents the activation function, FC is the fully connected layer, DW is the depth wise convolution. UNet 3+ improves lesion segmentation by leveraging nested skip pathways to capture features at multiple scales, which enhances its ability to identify lesions of different sizes and shapes. It ensures that intermediate layers actively contribute to the learning process, accelerating convergence and reducing the risk of overfitting, particularly when working with limited medical image data. Its capacity to extract fine-grained details while preserving global context makes the model more robust to noise, artifacts commonly found in dermoscopic images, lead to more reliable segmentation in real-world clinical scenarios. It is given in Eq. (9),

$$A_{j,i} = \frac{\exp(N_j \cdot M_i)}{\sum_{j=1}^{m}\exp(N_j \cdot M_i)} \tag{9}$$

where, $A_{j,i}$ is measures impact of i^{th} location on j^{th} location, m is the number of pixel values. The architecture diagram of HDAETUNet3+ is represented in Fig. 2.

The HDAETUNet3+ architecture is designed for dermoscopic image segmentation, focusing on accurately segmenting regions of interest in dermoscopic images. It features a dual-transformer block structure, with skip connections and self-supervised contrastive learning to improve feature representation. The encoder extracts features progressively through patch merging and dual-transformer blocks, while the decoder upsamples and refines the segmentation mask. The network also incorporates full-scale intra- and inter-skip connections and ground truth supervision to guide the learning process. This sophisticated design aims to provide precise and reliable segmentation of ROIs in dermoscopic images, supporting the diagnosis of skin conditions. Then the each position of the image is given in Eq. (10).

$$GSA(N,M,W)_q = \sum_{p=1}^{h\times w}\left(W_p B_{q,p}\right) \tag{10}$$

Here $GSA(N,M,W)_q$ are features to generate the output image Finally, HDAETUNet3+ is used to segment the ROI region. Segmentation output is given into classification phase.

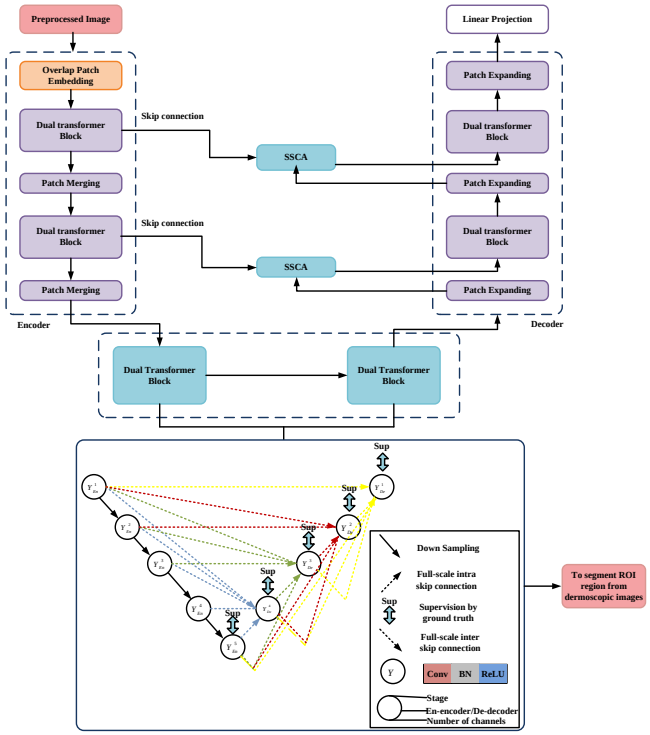

Fig. 2. Architecture of HDAETUNet3+.

D. Classification utilizing Dynamic Graph Convolutional Recurrent Imputation Network

The classification using DGCRIN is categorizing skin lesion such as actinic keratosis, Dermatofibroma, Basal cell carcinoma, benign keratosis, vascular lesion, Squamous cell carcinoma Melanocytic nevus, Melanoma [32]. The architecture diagram of DGCRIN is represented in Fig. 3. The DGCRIN captures the evolving relationships between image points over time, enabling it to adapt to changes in the image structure. The recurrent component adds temporal context, helping the model learn sequential patterns and enhance prediction accuracy, particularly when dealing with incomplete image. By incorporating imputation techniques, the model can effectively manage missing, leading to more robust and

accurate classification results. DGCRIN utilizes Graph Convolutional Networks to capture spatial dependencies within graph-structured image, making it particularly effective for datasets where the relationships between nodes are crucial for understanding missing data patterns. By incorporating both spatial and temporal information, DGCRIN can learn richer, more comprehensive representations of the image. Its ability to adapt to both spatial and temporal complexities enables it to handle intricate image patterns, making it especially well-suited for imputation tasks where the connections between missing values are complex and non-linear. The architecture diagram illustrates the DGCRIN model, where the input to the process is a set of segmented images. The model consists of three main components: a masked GRU, a DGCGRU, and a graph generator. The graph generator dynamically creates a graph at every time step to denote the geographical correlations of the road network, using both historical data and the current imputed data. The DGCGRU effectively captures the spatiotemporal relationships in the data by integrating the dynamic graph with a static graph and replacing the fully connected layers in a conventional GRU with a dynamic graph convolution operation. Additionally, a masked GRU is employed to independently analyze the masking matrix and identify patterns in the missing data. The information is then combined by a fusion layer using a temporal decay mechanism, and data inference is performed by a fully connected layer. This iterative process helps the model achieve high accuracy in classifying skin lesions. Thus, network layers are part of the recurrent imputation network model calculated as given in Eq. (11),

$$G_{E,t} = \tanh\left(V_E\left(G_{A,t}\Theta\tilde{G}_{m,t}\right) + y_E\right) \tag{11}$$

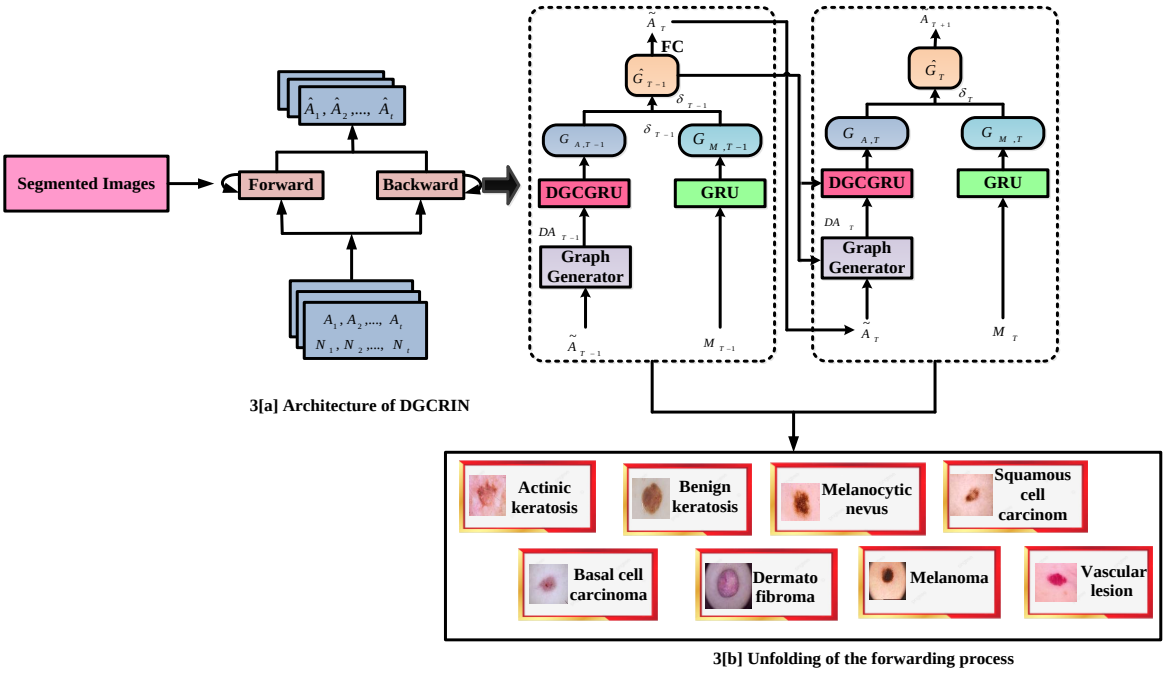

Fig. 3. (a) Architecture diagram of DGCRIN and (b) Unfolding of the forward process.

where, indicates the observation of each features, represents the significance of observation, indicates the hidden state, indicates the exponential function, indicates the sigmoid multiplication, indicates the constantly updated value, and represents the squared random initialization value. To classify the actinic keratosis, Basal cell carcinoma can be expressed as given in Eq. (12).

$$\lambda_t = \frac{1}{f^{\max}\left(0, V_\lambda \delta_t + y_\lambda\right)} \tag{12}$$

Here λ_t represents the efficient reconstruction value, δ_t represents the learnable variable, V_λ represents the forward along backward feature matrices, y_λ represents the activation functions and $f^{\max}$ depicts at each time step. To classify the benign keratosis, dermatofibroma, and melanocytic nevusis, the calculation is performed as given in Eq. (13).

$$A_{T+1} = V_A \hat{G}_t + y_A \tag{13}$$

In Eq. (13), the term B_{T+1} represent the estimated value, V_A denotes the scoring vector, $\hat{G}_t$ is the dynamic adjacency matrix is regularized by the activation function and y_A indicates the learnable parameter. To classify the Melanoma, Squamous cell carcinoma, vascular lesion is calculated as given in Eq. (14),

$$A_{T+1} = A_{T+1}\Theta N_{T+1} + \tilde{A}_{T+1}\Theta\left(1 - N_{T+1}\right) \tag{14}$$

where, A_{T+1} represents the prediction value, $\tilde{A}_{T+1}$ represents the image consumption, Θ indicates the sigmoid multiplication operator, and N_{T+1} denotes the SCC. Finally, the DGCRIN classified the skin lesion likes SCC, AK, BCC, Dermatofibroma, Melanoma, vascular lesion, Melanocytic nevus, benign keratosis. The RBBMOA is utilized to optimize

DGCRIN optimal parameter y_a and δ_t. The RBBMOA is used for tuning DGCRIN weight, bias parameter.

E. Optimization using Red Billed Blue Magpie Optimization Algorithm

The weights parameter y_a and δ_t of proposed DGCRIN is optimized utilizing the proposed Red Billed Blue Magpie Optimization Algorithm (RBBMOA) [33].This optimizer works efficiently and quickly, converging to the optimal weight parameters in a shorter time than other optimization techniques. It optimizes network parameters, leading to improved model performance and higher classification accuracy for skin lesion detection. The RBBMOA refines the standard algorithm by introducing a more effective, reducing the risk of getting trapped in local minima. It also quicker convergence and improved solution accuracy. Furthermore, RBBMOA adjusts dynamically to complex problem environments, enhancing its efficiency across various optimization tasks. As foraging, it uses mix of ground-walking, jumping, searching along branches to find food. It also stores food for later consumption. To protect its cached items from theft by other an also there wise birds; it hides food in secure locations such as tree hollows, forks, and rock crevices. Overall, it is versatile predator, employing various strategies to acquire and store food. It also displays social behavior and cooperation when hunting. The flowchart illustrating the proposed RBBMOA approach is presented in Fig. 4.

1) Stepwise procedures for RBBMOA: The step by step technique is defined to obtain optimal value of DGCRIN dependent on RBBMOA. At first, RBBMOA makes evenly allocating populace to enhance parameter of DGCRIN.

Step 1: Initialization

The initialization phase of RBBMOA applicant solutions is created smoothly within the constraints of a given problem, requiring updates after iteration. It is given in Eq. (15),

$$Y = \begin{bmatrix} y_{1,1} & \cdots & y_{1i} & y_{1,\dim-1} & y_{1,\dim} \\ y_{2,1} & \cdots & y_{2,i} & \cdots & y_{2,\dim} \\ \cdots & \cdots & y_{j,i} & \cdots & \cdots \\ \cdots & \cdots & \cdots & \cdots & \cdots \\ y_{m-1,1} & \cdots & y_{m-1,i} & \cdots & y_{m-1,\dim} \\ y_{m,1} & \cdots & y_{m,i} & y_{m,\dim-1} & y_{m,\dim} \end{bmatrix} \quad (15)$$

where, Y signifies location of search agent, $\dim$ denotes dimension of solving problem, m represents population size.

Step 2: Random Generation

Input parameters are generated randomly. Optimal fitness values are preferred depending upon explicit hyper parameter situation.

Step 3: Fitness function

A random solution is generated utilizing initialized assessments using factor optimization value; it is evaluated for optimizing weight parameter y_a and δ_t of skin lesion. It is given in Eq. (16),

$$Fitness\ Function = optimize\ (y_a\ \&\ \delta_t) \quad (16)$$

where, y_a is utilized to increasing accuracy, δ_t is utilized to decreasing error rate.

Step 4: Search for food

To enhance efficiency, red-billed blue magpies typically hunt in small groups. It uses various techniques, including walking, jumping on ground, scouring trees for food resources. Billed blue magpies use adaptable hunting strategies that depend on environmental conditions, resources at hand, ensure adequate food supply as shown in Eq. (17).

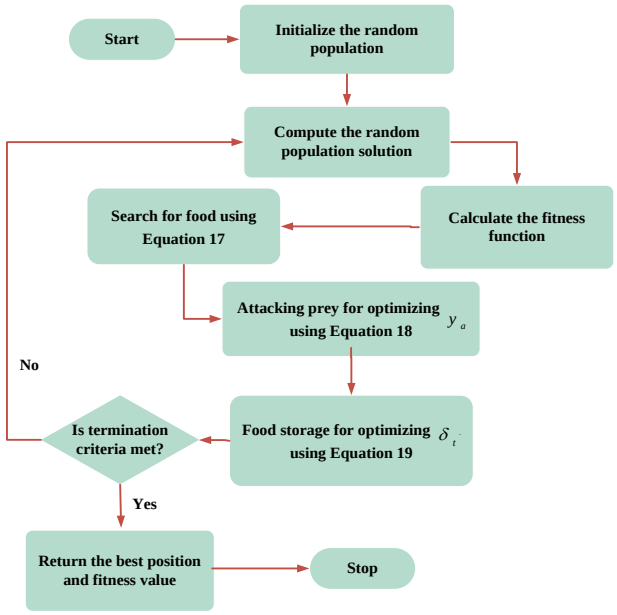

Fig. 4. Flowchart of RBBMOA for optimizing DGCRIN parameter.

$$Y^j(l+1) = Y^j(l) + \left(\frac{1}{q} \times \sum_{n=1}^{q} Y^n(l) - Y^{sa}(l)\right) \times Rand_2 \quad (17)$$

where, $Y^j(l+1)$ represents the prey attackers, Y^j represents the normal distribution, l represents the hunting behaviour, q indicates red-billed blue magpies typically hunt within small groups, Y^n represents the tactics, $Y^{sa}(l)$ denotes randomly selected search agents for current iteration, $Randn_2$ denotes random number 2.

Step 5: Attacking prey for optimizing y_a

When pursuing prey, red-billed blue magpie demonstrates higher degree of hunting skill, teamwork. It uses fast picking, jumping, and flying to grab insects, among other strategies. Typically, small prey or plants are the main focus of small group operations. Red-billed blue magpies can work together to pursue larger prey, such as tiny animals or large insects, when they are in groups. It is expressed as Eq. (18).

$$Y^j(l+1) = Y^{food}(l) + DG \times y_a \left(\frac{1}{q} \times \sum_{n=1}^{q} Y^n(l) - Y^j(l) \right) \times Randn_1 \quad (18)$$

where, Y^{food} represents the position of the food, DG represents the diverse strategies, and $Randn_1$ denotes random number 1 and y_a is used to increase the accuracy.

Step 6: Food storage for optimizing δ_t

Red-billed blue magpies not only hunt and fight prey, but it also stockpile extra food in tree holes and other hidden places so they may eat it later, providing a consistent source of food even in times of famine. This procedure saves information about the solutions, making it easier for people to find the value that is globally optimal. It is given in Eq. (19).

$$Y^j(l+1) = \delta_t \begin{cases} Y^j(l) & if \ \ fitness^j_{old} > fitness^j_{new} \\ Y^j(l+1) & else \end{cases} \quad (19)$$

where, $fitness^j_{old}$ and $fitness^j_{new}$ denotes fitness values earlier than, following position modernize of j^{th} red-billed blue magpie, δ_t is used for decreasing the error rate.

Step 7: Termination

The weight parameter value of creator y_a and δ_t from DGCRIN is improved by RBBMOA; it repeat step 3 until it acquires its halting criteria $Y = Y + 1$. Then, the SLCDI-DGCRIN-RBBMOA methods effectively classify the skin lesion by higher accuracy and low error rate.

2) Complexity analysis: The RBBMOA algorithm is based on two key components: solution initialization with the primary approach functions, which include computing the fitness values and update the solutions. Let n represent the cout of search agents, T denote the maximal count of iterations, and $\dim$ refer to the problem's dimension. Finding the optimal location and updating the location of every solutions are included in the solution updating process, which has a computational difficulty of $O(T \times n) + O(2 \times T \times n \times \dim)$, while the solution initialization process has a computational complexity of $O(n)$. As a result, the overall computational complexity of the proposed RBBMOA algorithm is $O(n \times T \times (2 \times \dim + 1))$.

IV. Result and Discussion

The experimental results of the proposed SLCDI-DGCRIN-RBBMOA approach is implemented in Python utilizing PC along Intel Core i5, 16GB RAM, 3.2 GHz CPU, Windows7, examined utilizing various performance measures likes accuracy, specificity, recall, precision, F1-score, computation time, error rate. The SLCDI-DGCRIN-RBBMOA model is tested against several performance metrics. Attained result of SLCDI-DGCRIN-RBBMOA approach is compared with existing methods likes DNN-EAI-SLC, MSLC-CNN-OIF, CSC-DI-DCNN respectively. Fig. 5 depicts the skin lesion classification workflow across different dermoscopic images, from segmented images, raw input images and pre-processed. Every modality captures exclusive anatomical details, which give to exact skin lesion detection.

A. Performance Measures

Performance metric accuracy, recall, specificity, F1-score, precision, computational time and error rate are examined for performance matrices. To measure performance metrics, performance matrix is required. Next matrixes are necessary to measure performance metrics.

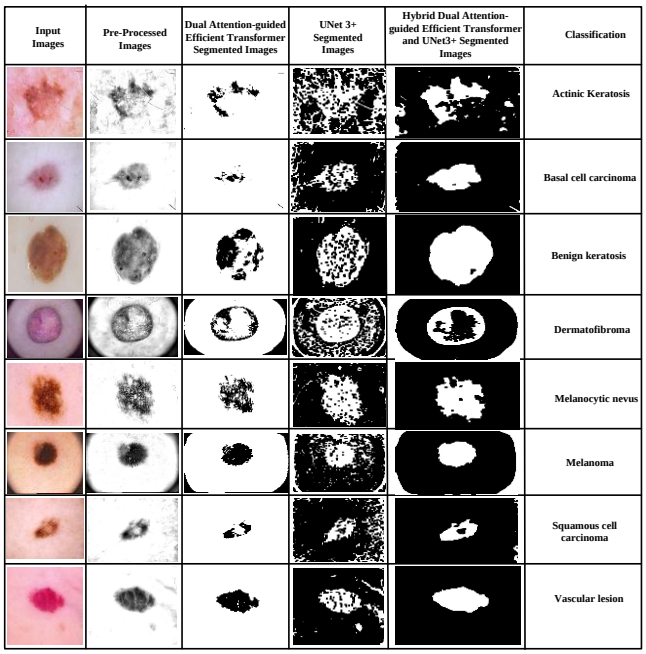

Fig. 5. Output of the proposed SLCDI-DGCRIN-RBBMOA method.

- True Positives: The number of actual positive cases that are accurately categorized as positive.
- True Negatives: The number of actual negative cases that are accurately categorized as negative.
- False Positives: The number of actual negative cases that are inaccurately classified as positive.
- False Negatives: The number of actual negative cases that are inaccurately classified as negative.

1) Accuracy: It is known as percentage of correctly identified cases among total instances and it is evaluated by Eq. (20),

$$Accuracy = \frac{TP + TN}{TP + TN + FP + FN} \quad (20)$$

2) Precision: It assess the capacity of model for recognize positive instances accurately out of all predicted instances cases, which is estimated by Eq. (21),

$$\Pr ecision = \frac{TP}{(TP + FP)} \quad (21)$$

3) Recall: It is measured through separating total count of elements in positive class with count of real positives and determined by Eq. (22),

$$\text{Re}call = \frac{TP}{(TP + FN)} \tag{22}$$

4) Specificity: The percentage of true negatives that approach exactly recognizes is known as specificity, it is exhibits in Eq. (23),

$$Specificity = \frac{TN}{TN + FP} \tag{23}$$

5) F1-score: It represents ensemble mean of precision, recall. It is calculated using Eq. (24),

$$F1 - score = 2 * \frac{precision * recall}{precision + recall} \tag{24}$$

6) Error rate: It is a statistic used to express the prediction inaccuracy of the methodology depending on the actual approach. This is scaled in Eq. (25),

$$Error\ \ Rate = 100 - Accuracy \tag{25}$$

B. Performance Measures

Fig. 6-14 shows simulation result of SLCDI-DGCRIN-RBBMOA method. The performance measures are analyzed with existing DNN-EAI-SLC, MSLC-CNN-OIF, and CSC-DI-DCNN methods. The analysis of accuracy performance is portrayed in Fig. 6. The graph-based design's superior ability to capture local interactions between features enhances prediction accuracy and minimizes misclassifications. Furthermore, modern optimization techniques refine the models tuning, resulting in improved accuracy in identifying actual cases of skin lesion. Here, SLCDI-DGCRIN-RBBMOA method attains 21.51%, 12.38%, and 24.61% higher accuracy for actinic keratosis; 16.26%, 14.05%, 19.51% greater accuracy for Basal cell carcinoma; 26.21%, 20.65%, 22.31% greater accuracy for benign keratosis; 41.79%, 20.25%, 15.85% greater accuracy for Dermatofibroma; 25.21%, 30.65%, 20.45% greater accuracy for Melanocytic nevus; 10.56%, 27.56%, 19.67% higher accuracy for Melanoma; 18.78%, 30.45%, and 29.67% higher accuracy for Squamous cell carcinoma; 28.78% higher accuracy for vascular lesion; analyzed with existing techniques such as DNN-EAI-SLC, MSLC-CNN-OIF, and CSC-DI-DCNN respectively.

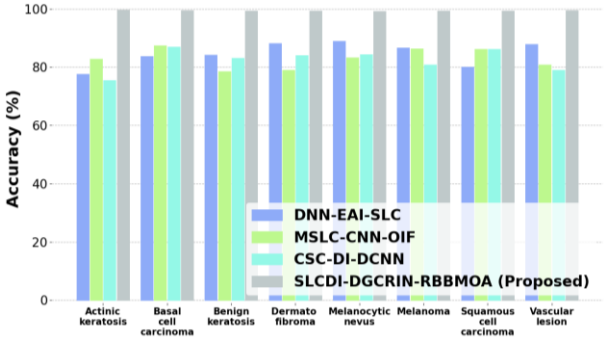

Fig. 6. Analysis of accuracy performance.

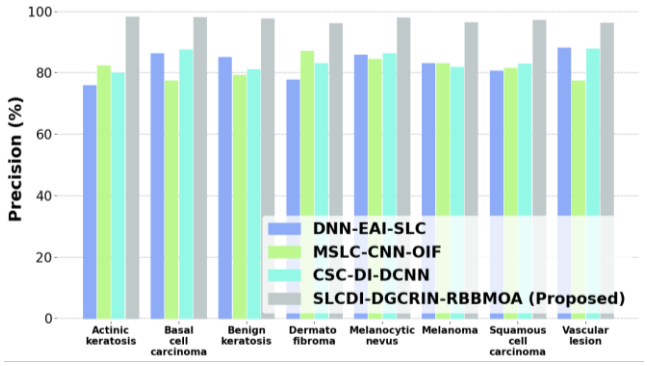

Fig. 7. Analysis of precision performance.

When compared to existing methods, the graph in Fig. 7 shows that SLCDI-DGCRIN-RBBMOA achieves higher precision across most skin lesion types due to model parameter optimization using the RBBMOA. This improvement in precision results from methods ability to better distinguish among different types of skin lesion. The enhanced accuracy is reflected in the methods overall performance, demonstrating its efficiency in managing and mitigating skin lesion. Here, SLCDI-DGCRIN-RBBMOA method attains 28%, 50%, and 21.51% higher Precision for actinic keratosis; 41.79%, 20.25%, 15.85% higher Precision for Basal cell carcinoma; 20.21%, 30.65%, and 28.31% higher precision for benign keratosis; 30.78%, 28.45%, and 29.56% higher precision for Dermatofibroma; 10.56%, 18.2%, and 16.46% higher precision for Melanocytic nevus; 29.59%, 30.89%, and 38.56% higher precision for Melanoma; 30.89%, 29.35%, and 29.89% higher precision for Squamous cell carcinoma; 29.50%, 26.40%, 30.67% greater precision for vascular lesion; analyzed with existing techniques likes DNN-EAI-SLC, MSLC-CNN-OIF, and CSC-DI-DCNN correspondingly.

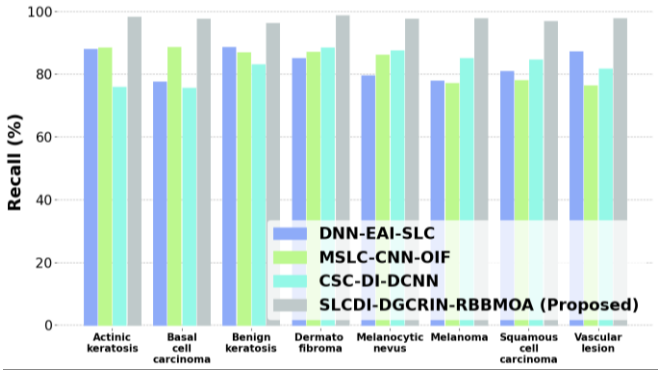

Fig. 8. Analysis of recall performance.

The model's high recall in SLCDI-DGCRIN-RBBMOA is attributed to its ability to effectively identify positive cases which is shown in fig. 8. By capturing intricate relationships between features, DGCRIN ensures that cases indicators are not overlooked. Additionally, RBBMOA optimizes the model's parameters to enhance sensitivity and increase the number of true positives identified. This combination strengthens the model's robustness against false negatives, reducing the number of missed examples and thereby improving recall. The SLCDI-DGCRIN-RBBMOA method attains 23.07%, 41.17%, and 24.67% higher recall for actinic keratosis; 43.47%,

25.31%, 16.47% higher recall for Basal cell carcinoma; 26.21%, 20.65%, and 22.31% higher recall for benign keratosis; 20.78%, 30.78%, and 12.56% higher recall for Dermatofibroma; 20.56%, 30.2%, and 28.46% higher recall for Melanocytic nevus; 30.29%, 35.89%, and 20.56% higher recall for Melanoma; 15.89%, 17.35%, and 29.46% higher recall for Squamous cell carcinoma; 30.26%, 20.46%, and 39.67% higher recall for vascular lesion; analyzed with existing techniques likes DNN-EAI-SLC, MSLC-CNN-OIF, and CSC-DI-DCNN.

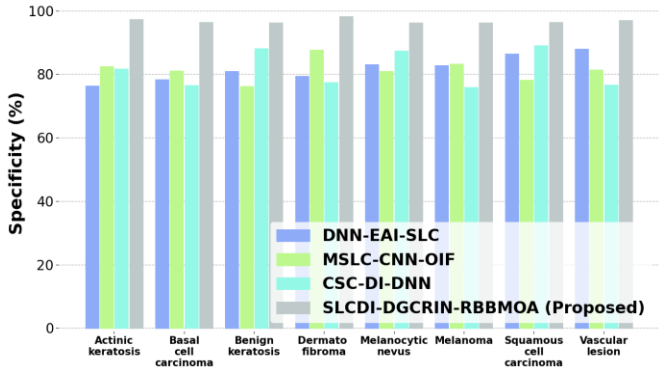

Fig. 9. Analysis of specificity performance.

Fig. 9 portrays the analysis of specificity performance. The specificity curve of a well-performing model will be lower at first and progressively higher as training goes on. The SLCDI-DGCRIN-RBBMOA method attains 17.75%, 24.55% and 12.66% high specificity for actinic keratosis; 21.01%, 14.08% and 17.33% high specificity for Basal cell carcinoma; 16.41%, 29.65%, and 24.31% higher specificity for Benign keratosis; 20.41%, 30.25%, and 14.83% higher specificity for Dermatofibroma; 29.41%, 30.48%, and 20.40% higher specificity for Melanocytic nevus; 17.01%, 29.08% and 30.67% higher specificity for Melanoma; 10.40%, 28.30% and 20.33% higher specificity for Squamous cell carcinoma; 29.59%, 20.9%, 25.31% greater specificity for Vascular lesion, analyzed with existing DNN-EAI-SLC, MSLC-CNN-OIF, and CSC-DI-DCNN models.

A model is considered to be comprehensive in recognizing all relevant cases and precise in forecasting positive cases if it's F1-score is higher. A high F1-score for the meningioma would propose that the system successfully detects critical circumstances without generating an excessive count of false alarms in context of skin lesion classification. Fig. 10 displays the analysis of F1-score performance. The SLCDI- DGCRIN-RBBMOA method attains 10.30%, 17.10% and 30.26% higher F1-score for the actinic keratosis; 28.02%, 11.56% and 13.67%.

F1-score for Basal cell carcinoma; 20.15%, 19.55%, and 12.21% high F1-score for Benign keratosis; 28.67%, 30.67%, and 23.67% high F1-score Dermatofibroma; 30.19%, 20.78%, and 20.56% higher F1-score for Melanocytic nevus; 29.68%, 10.56%, 26.67% greater F1-score for Melanoma; 29.78%, 10.56%, 30.56% greater F1-score for Squamous cell carcinoma; 20.67%, 17.49%, and 30.92% larger F1-score for Vascular lesion; compared with existing DNN-EAI-SLC, MSLC-CNN-OIF, and CSC-DI-DCNN models.

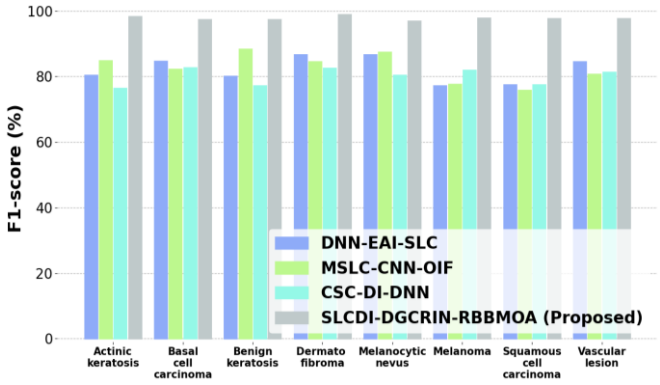

Fig. 10. Analysis of F1-score

Fig. 11 shows the analysis of computational time performance. It is faster due to optimized training methods, which include advanced optimization algorithms and effective hyperparameter tuning, reducing the number of training iterations required. Additionally, the spatio-temporal nature of DGCRIN allows for the parallel handling of spatial and temporal features, further enhancing computational efficiency. The proposed SLCDI-DGCRIN-RBBMOA method attains 15.01%, 13.44%, 14.27% lower computational time; analyzed with existing DNN-EAI-SLC, MSLC-CNN-OIF, and CSC-DI-DCNN methods.

A decreased error rate suggests improved model performance. Fig. 12 shows performance of error rate analysis.

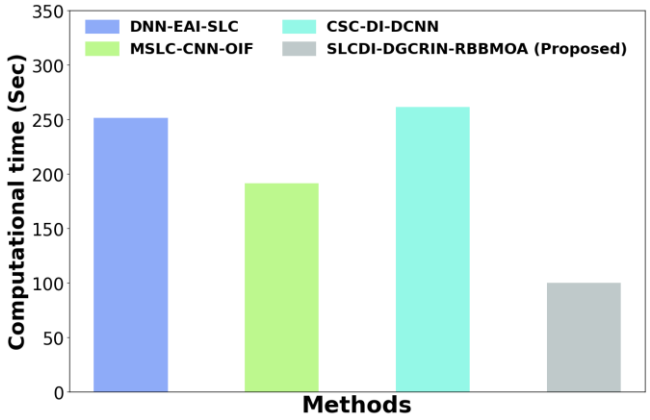

Fig. 11. Analysis of computational time performance.

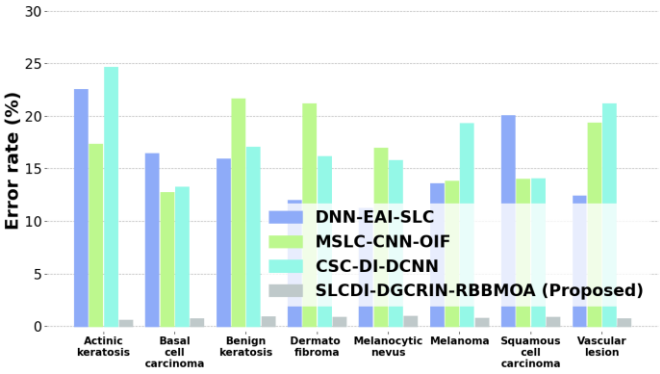

Fig. 12. Error rate analysis.

SLCDI-DGCRIN-RBBMOA has a significantly lower error rate than these existing methods, it indicates that the optimization techniques and advanced model architecture used in DGCRIN effectively reduce misclassifications, improving overall accuracy in identifying various skin lesion types. This reduction in error rates illustrates the new model's capacity to improve skin lesion classification reliability. Here, SLCDI-DGCRIN-RBBMOA method attains15.85%, 23.37%, and 22.04% lower Error rate for actinic keratosis; 25.97%, 20.57%, 19.23% lower Error rate for Basal cell carcinoma;24.78%, 22.67%, and 30.46% lower Error rate for benign keratosis; 30.79%, 10.29%, 25.59% lower error rate for Dermatofibroma; 20.45%, 25.89%, and 30.57% lower error rate for Melanocytic nevus; 19.67%, 30.16%, and 20.45% lower error rate for Melanoma; 20.67%, 30.15%, and 30.10% lower error rate for Squamous cell carcinoma; 15.79%, 20.56%, and 12.18% low error rate for vascular lesion; analyzed with existing approaches such as DNN-EAI-SLC, MSLC-CNN-OIF, and CSC-DI-DCNN correspondingly.

The Computational Complexity of the proposed SLCDI-DGCRIN-RBBMOA approach increases with increasing input size, indicating its scalability and appropriateness for bigger datasets. This graph in Fig. 13 highlights how much faster the SLCDI-DGCRIN-RBBMOA to the existing techniques likes DNN-EAI-SLC, MSLC-CNN- OIF and CSC-DI-DCNN respectively. Here, when the input size increases then the CPU operation decreases gradually. Fig. 14 depicts the confusion matrix.

C. Comparative Analysis of Proposed Approach

Table II presents a segmentation comparison with other methods depending upon accuracy, precision, recall, and F1-score. ResNet 50 shows an accuracy of 70.7%, with a strong recall of 86.6%, but a lower precision of 76.8%. DarkNet19 has higher accuracy but struggles with lower precision and recall. EfficientNet offers a well-balanced performance, achieving 79.5% accuracy, high precision, and moderate recall. Both the Dual Swin Transformer and Dual Vision Transformer perform well in recall; but both models have lower precision. The Dual Attention-guided Efficient Transformer shows good precision but lower recall. UNet3+ delivers strong results across all metrics, with an accuracy of 84.6%. The proposed Hybrid Dual Attention-guided Efficient Transformer and UNet 3+ model stands out with exceptional results, achieving 99.4% accuracy, 92.9% precision, 94.5% recall, and 95.4% F1-score, making it the most effective model in segmentation.

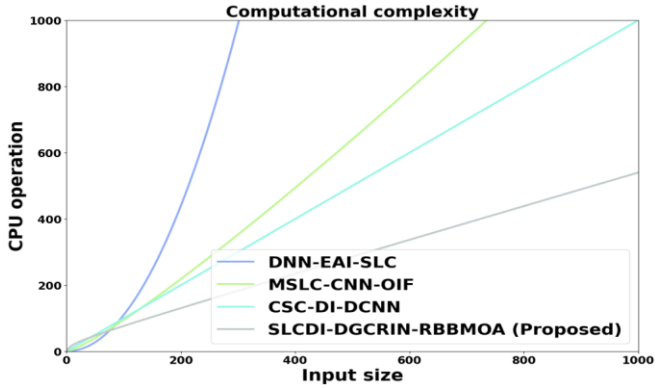

Fig. 13. Computational complexity performance analysis.

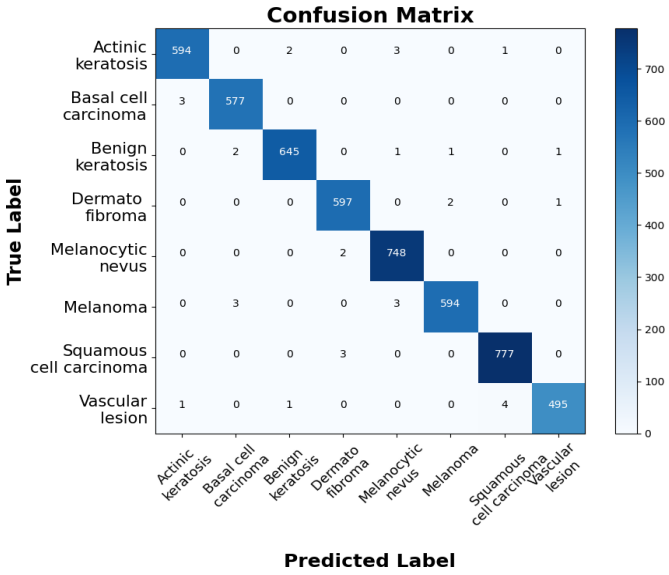

Fig. 14. Confusion matrix analysis.

TABLE II. SEGMENTATION COMPARISON WITH OTHER MODELS

Models	Accuracy	Precision	Recall	F1-score
ResNet 18 [21]	70.7%	76.8%	86.6%	80.3%
DarkNet19 [22]	75.4%	70.1%	67.3%	82.4%
EfficientNet [23]	79.5%	87.9%	72.6%	80.7%
Dual Swin Transformer [34]	76.4%	70.3%	74.9%	79.4%
Dual Vision Transformer [35]	80.2%	76.9%	85.2%	71.5%
Dual Attention-guided Efficient Transformer [30]	79.7%	80.1%	72.9%	67.8%
UNet3+ [31]	84.6%	79.9%	83.2%	80.6%
Hybrid Dual Attention-guided Efficient Transformer and UNet 3+ (Proposed) [30, 31]	99.4%	92.9%	94.5%	95.4%

TABLE III. COMPARATIVE ANALYSIS OF PROPOSED APPROACH

Methods	Accuracy (%)	Precision (%)	Recall (%)	Specificity (%)	F1-score (%)	Computational time (sec)	Error rate (%)
DNN-EAI-SLC [21]	77.47	75.69	87.80	76.22	80.37	250	22.52
MSLC-CNN-OIF [22]	82.70	82.20	88.26	82.30	84.82	190	17.29
CSC-DI-DCNN [23]	75.35	79.85	75.75	81.55	76.45	260	24.64
RDCNN-SLC-MFCC [24]	83.59	86.15	77.48	78.22	84.64	240	16.40
DCNN-SLMC-GAPI [25]	86.32	77.32	88.46	80.94	82.15	150	12.72
CNN-SLC-SH [26]	86.76	87.32	75.75	76.40	82.58	180	13.23
GAN-HMC [27]	84.08	85.20	88.45	80.75	80.01	230	15.91
SLCDI-DGCRIN-RBBMOA (proposed)	99.16	98.16	98.11	97.20	98.27	99	0.592

Table III provides a comparative analysis of SLCDI-DGCRIN-RBBMOA method alongside several other existing methods based on key performance metrics, comprising specificity, accuracy, precision, recall, F1-score, computational time, and error rate. Among the methods evaluated, the proposed SLCDI-DGCRIN-RBBMOA approach outperforms the others, achieving the highest accuracy and strong results across each metrics, like specificity, precision, recall, and F1-score. Additionally, it boasts the lowest error rate and computational time compared to the other methods. In contrast, approaches such as DNN-EAI-SLC, CSC-DI-DCNN, and RDCNN-SLC-MFCC exhibit lower accuracy and higher error rates, emphasizing the superior efficiency and effectiveness of the proposed model. This comparison emphasizes the exceptional performance with effectiveness of the SLCDI-DGCRIN-RBBMOA approach.

D. Discussion

The proposed model for Skin Lesions Classification in Dermoscopic Images employs an Optimized Dynamic Graph Convolutional Recurrent Imputation Network (DGCRIN) to enhance classification performance. The methodology begins with preprocessing, utilizing Confidence Partitioning Sampling Filtering (CPSF) to remove noise, resize images, and enhance quality. This aligns with [29], who demonstrated that CPSF significantly improves feature extraction in medical imaging by preserving essential details while eliminating distortions. Following preprocessing, the Hybrid Dual Attention-guided Efficient Transformer and UNet3+ (HDAETUNet3+) is applied for segmentation. The efficiency of hybrid transformer-based segmentation models in medical imaging has been well-documented. The study in [30] proposed Dae-former, a dual attention-guided efficient transformer, demonstrating superior segmentation accuracy for medical images, which supports the effectiveness of HDAETUNet3+ in identifying precise lesion boundaries. Additionally, the integration of UNet3+ [31], which employs full-scale connectivity, further enhances segmentation performance, ensuring robust ROI extraction from dermoscopic images. For classification, Dynamic Graph Convolutional Recurrent Imputation Network (DGCRIN) is utilized. Research on graph convolutional networks in handling complex spatial dependencies supports the use of DGCRIN. The research in [32] demonstrated the effectiveness of dynamic graph convolutional networks in managing spatiotemporal dependencies, which is crucial for accurately classifying skin lesions with varying patterns and structures. Despite its advantages, the proposed model presents some limitations. One challenge is the computational demand of deep learning and optimization algorithms. As noted by study [33], optimization algorithms like the Red-Billed Blue Magpie Optimizer (RBBMOA) enhance accuracy but may require extensive computational resources, which could be a concern for real-time medical applications. Additionally, the model's complexity and fine-tuning requirements may pose challenges for clinical integration, a concern also raised in prior studies on deep learning-based skin lesion classification [2].

V. CONCLUSION

The SLCDI-DGCRIN-RBBMOA model achieves significant advancements in skin lesion detection and classification. Utilizing dermoscopic images from the ISIC-2019 dataset, the model incorporates CPSF for noise reduction, resizing, and image enhancement. The HDAETUNet3+ effectively segments the ROI, while DGCRIN classifies lesions, and RBBMOA optimizes DGCRIN, enhancing classification accuracy. This approach demonstrates superior performance, achieving 21.51%, 12.38%, and 21.51% higher accuracy, along with 15.85%, 23.37%, and 22.04% lower error rates compared to DNN-EAI-SLC, MSLC-CNN-OIF, and CSC-DI-DCNN, respectively. However, challenges such as image quality variability and overlapping lesion features remain areas for further exploration. Future research could explore applying skin lesion classification techniques, with a focus on addressing disputes like data variability, noise in medical imaging, and the need for real-time diagnosis. Incorporating advanced feature extraction techniques could enhance lesion detection accuracy and improve classification performance. Additionally, optimizing deep learning models for domain-specific tasks could lead to more reliable skin cancer detection and prognosis. Moreover, incorporating multi-modal data, such as clinical metadata (e.g., patient history and genetic factors), alongside dermoscopic images could improve diagnostic precision. Lastly, future research could focus on edge and mobile deployment, adapting the model for lightweight, resource-efficient implementations, making it accessible in remote and resource-limited areas.

REFERENCES

[1] Hosny, K.M., Said, W., Elmezain, M. and Kassem, M.A., 2024. Explainable deep inherent learning for multi-classes skin lesion classification. Applied Soft Computing, 159, p.111624.

[2] Khater, T., Ansari, S., Mahmoud, S., Hussain, A. and Tawfik, H., 2023. Skin cancer classification using explainable artificial intelligence on pre-

extracted image features. *Intelligent Systems with Applications*, *20*, p.200275.

[3] Hosny, K.M., Said, W., Elmezain, M. and Kassem, M.A., 2024. Explainable deep inherent learning for multi-classes skin lesion classification. *Applied Soft Computing*, *159*, p.111624.

[4] Jasil, S.G. and Ulagamuthalvi, V., 2023. A hybrid CNN architecture for skin lesion classification using deep learning. *Soft Computing*, pp.1-10.

[5] Maqsood, S. and Damaševičius, R., 2023. Multiclass skin lesion localization and classification using deep learning based features fusion and selection framework for smart healthcare. *Neural networks*, *160*, pp.238-258.

[6] Sulthana, R., Chamola, V., Hussain, Z., Albalwy, F. and Hussain, A., 2024. A novel end-to-end deep convolutional neural network based skin lesion classification framework. *Expert Systems with Applications*, *246*, p.123056.

[7] Deng, X., 2024. LSNet: a deep learning based method for skin lesion classification using limited samples and transfer learning. *Multimedia Tools and Applications*, pp.1-21.

[8] Alenezi, F., Armghan, A. and Polat, K., 2023. Wavelet transform based deep residual neural network and ReLU based Extreme Learning Machine for skin lesion classification. *Expert Systems with Applications*, *213*, p.119064.

[9] Ajmal, M., Khan, M.A., Akram, T., Alqahtani, A., Alhaisoni, M., Armghan, A., Althubiti, S.A. and Alenezi, F., 2023. BF2SkNet: Best deep learning features fusion-assisted framework for multiclass skin lesion classification. *Neural Computing and Applications*, *35*(30), pp.22115-22131.

[10] Bozkurt, F., 2023. Skin lesion classification on dermatoscopic images using effective data augmentation and pre-trained deep learning approach. *Multimedia Tools and Applications*, *82*(12), pp.18985-19003.

[11] Dillshad, V., Khan, M.A., Nazir, M., Saidani, O., Alturki, N. and Kadry, S., 2023. D2LFS2Net: Multi-class skin lesion diagnosis using deep learning and variance-controlled Marine Predator optimisation: An application for precision medicine. *CAAI Transactions on Intelligence Technology*.

[12] Tsai, W.X., Li, Y.C. and Lin, C.H., 2023. Skin lesion classification based on multi-model ensemble with generated levels-of-detail images. *Biomedical Signal Processing and Control*, *85*, p.105068.

[13] Arora, G., Dubey, A.K. and Jaffery, Z.A., 2023. Multiple skin lesion classification using deep, ensemble, and shallow (DEnSha) neural networks approach. *International Journal of System Assurance Engineering and Management*, *14*(Suppl 1), pp.385-393.

[14] Akram, A., Rashid, J., Jaffar, M.A., Faheem, M. and Amin, R.U., 2023. Segmentation and classification of skin lesions using hybrid deep learning method in the Internet of Medical Things. *Skin Research and Technology*, *29*(11), p.e13524.

[15] Asiri, Y., Halawani, H.T., Algarni, A.D. and Alanazi, A.A., 2023. IoT enabled healthcare environment using intelligent deep learning enabled skin lesion diagnosis model. *Alexandria Engineering Journal*, *78*, pp.35-44.

[16] Khan, M.A., Akram, T., Zhang, Y.D., Alhaisoni, M., Al Hejaili, A., Shaban, K.A., Tariq, U. and Zayyan, M.H., 2023. SkinNet-ENDO: Multiclass skin lesion recognition using deep neural network and Entropy-Normal distribution optimization algorithm with ELM. *International Journal of Imaging Systems and Technology*, *33*(4), pp.1275-1292.

[17] Golnoori, F., Boroujeni, F.Z. and Monadjemi, A., 2023. Metaheuristic algorithm based hyper-parameters optimization for skin lesion classification. *Multimedia Tools and Applications*, *82*(17), pp.25677-25709.

[18] Yang, Y., Xie, F., Zhang, H., Wang, J., Liu, J., Zhang, Y. and Ding, H., 2023. Skin lesion classification based on two-modal images using a multi-scale fully-shared fusion network. *Computer Methods and Programs in Biomedicine*, *229*, p.107315.

[19] Kaur, R. and Kaur, N., 2024. Ti-FCNet: Triple fused convolutional neural network-based automated skin lesion classification. *Multimedia Tools and Applications*, *83*(11), pp.32525-32551.

[20] QasimGilani, S., Syed, T., Umair, M. and Marques, O., 2023.Skin cancer classification using deep spiking neural network. *Journal of Digital Imaging*, *36*(3), pp.1137-1147.

[21] Nigar, N., Umar, M., Shahzad, M.K., Islam, S. and Abalo, D., 2022. A deep learning approach based on explainable artificial intelligence for skin lesion classification. *IEEE Access*, *10*, pp.113715-113725.

[22] Khan, M.A., Hamza, A., Shabaz, M., Kadry, S., Rubab, S., Bilal, M.A., Akbar, M.N. and Kesavan, S.M., 2024. Multiclass skin lesion classification using deep learning networks optimal information fusion. *Discover Applied Sciences*, *6*(6), pp.1-13.

[23] SM, J., P, M., Aravindan, C. and Appavu, R., 2023. Classification of skin cancer from dermoscopic images using deep neural network architectures. *Multimedia Tools and Applications*, *82*(10), pp.15763-15778.

[24] Alsahafi, Y.S., Kassem, M.A. and Hosny, K.M., 2023. Skin-Net: a novel deep residual network for skin lesions classification using multilevel feature extraction and cross-channel correlation with detection of outlier. *Journal of Big Data*, *10*(1), p.105.

[25] Raghavendra, P.V., Charitha, C., Begum, K.G. and Prasath, V.B.S., 2023. Deep Learning–Based Skin Lesion Multi-class Classification with Global Average Pooling Improvement. *Journal of Digital Imaging*, *36*(5), pp.2227-2248.

[26] Rezaee, K. and Zadeh, H.G., 2024. Self-attention transformer unit-based deep learning framework for skin lesions classification in smart healthcare. *Discover Applied Sciences*, *6*(1), p.3.

[27] Thanka, M.R., Edwin, E.B., Ebenezer, V., Sagayam, K.M., Reddy, B.J., Günerhan, H. and Emadifar, H., 2023. A hybrid approach for melanoma classification using ensemble machine learning techniques with deep transfer learning. *Computer Methods and Programs in Biomedicine Update*, *3*, p.100103.

[28] https://www.kaggle.com/datasets/mdefajalam/isic-2019-skin-disease

[29] Qiang, X., Xue, R. and Zhu, Y., 2024. Confidence partitioning sampling filtering. *EURASIP Journal on Advances in Signal Processing*, *2024*(1), p.24.

[30] Azad, R., Arimond, R., Aghdam, E.K., Kazerouni, A. and Merhof, D., 2023, October. Dae-former: Dual attention-guided efficient transformer for medical image segmentation. In *International Workshop on PRedictive Intelligence InMEdicine* (pp. 83-95). Cham: Springer Nature Switzerland.

[31] Zhao, B., Tang, P., Luo, X., Li, L. and Bai, S., 2022. SiUNet3+-CD: A full-scale connected Siamese network for change detection of VHR images. *European Journal of Remote Sensing*, *55*(1), pp.232-250.

[32] Kong, X., Zhou, W., Shen, G., Zhang, W., Liu, N. and Yang, Y., 2023. Dynamic graph convolutional recurrent imputation network for spatiotemporal traffic missing data. *Knowledge-Based Systems*, *261*, p.110188.

[33] Fu, S., Li, K., Huang, H., Ma, C., Fan, Q. and Zhu, Y., 2024. Red-billed blue magpie optimizer: a novel metaheuristic algorithm for 2D/3D UAV path planning and engineering design problems. *Artificial Intelligence Review*, *57*(6), pp.1-89.

[34] Lin, A., Chen, B., Xu, J., Zhang, Z., Lu, G. and Zhang, D., 2022. Ds-transunet: Dual swin transformer u-net for medical image segmentation. *IEEE Transactions on Instrumentation and Measurement*, *71*, pp.1-15.

[35] Yao, T., Li, Y., Pan, Y., Wang, Y., Zhang, X.P. and Mei, T., 2023. Dual vision transformer. *IEEE transactions on pattern analysis and machine intelligence*, *45*(9), pp.10870-10882.